Pure Appl. Chem., Vol. 79, No. 5, pp. 825–850, 2007.
doi:10.1351/pac200779050825

Solubility of salts in water: Key issue for crystal growth and dissolution processes*

Petros G. Koutsoukos‡, Aikaterini N. Kofina, and Dimitra G. Kanellopoulou

Department of Chemical Engineering, University of Patras and Foundation of Research and Technology Hellas, Institute of Chemical Engineering and High Temperature Chemical Processes, GR26504 Patras, Greece

Abstract: The formation of sparingly soluble salts from aqueous solutions and their dissolution has attracted broad research interest. Of particular importance is the formation and transformation of minerals exhibiting polymorphism or encountered in more than one crystalline phase as, for example, in the case of calcium phosphates, formed in biological mineralization and in industrial-scale deposits. Understanding of these processes depends primarily on the equilibrium between the mineral phases considered and the aqueous medium in contact. Precipitation takes place in supersaturated solutions with rates depending on the solution supersaturation. The experimental investigation may reveal mechanistic details if done at sustained supersaturation. The kinetics of crystal growth depends either on surface diffusion or on bulk diffusion, which in turn is controlled by the medium fluid dynamics. In the case of magnesium ammonium phosphate (struvite), the presence of water-soluble organic compounds is responsible for the retardation both of the time needed for the onset of precipitation and for the kinetics of growth of the supercritical nuclei. Dissolution processes are controlled by the same mechanisms. In the case of calcitic marble, the dissolution in alkaline solutions is controlled by surface diffusion. Compounds active at the marble/water interface may in this case be used as protective agents.

Keywords: crystal growth; dissolution, kinetics of; dissolution, inhibition of; calcium phosphate; struvite, solubility of; calcite; Carrara marble.

INTRODUCTION

Life on Earth (and most probably in the Universe) is bound with aqueous solutions and connected with their physics and chemistry. Solutions in connection with dissolved salts may be classified as:

a. Saturated, containing maximum amount of solute that can be dissolved at the conditions of the solution. Once no more solute will dissolve, the solution is said to be saturated.
b. Undersaturated, in which less solute than the maximum amount possible is dissolved. Once more solute is added, it will dissolve.
c. Supersaturated, which holds more dissolved solute than it is possible for a saturated solution at the same conditions (honey is a supersaturated solution of sugar).

*Paper based on a presentation at the 12th International Symposium on Solubility Phenomena and Related Equilibrium Processes (ISSP-12), 23–28 July 2006, Freiberg, Germany. Other presentations are published in this issue, pp. 825–894.
‡Corresponding author

Super- and undersaturated solutions are not in equilibrium with the solid phase, and this condition is established by precipitation and dissolution, respectively, of the corresponding salt. Precipitation processes from aqueous physiological fluids are particularly significant in this respect: crystallization, that is, the nucleation and growth of crystals and, subsequently, their possible dissolution. Crystallization from solutions is thermodynamically determined by the solubility of crystallizing components and kinetically by fluidity and the processes of diffusion in the initial phase. Depending on the solubility of the mineral phases, the supersaturation with respect to a particular crystalline phase is determined on the basis of the detailed knowledge of solution speciation. Changes in solution supersaturation may be the result of concomitant processes (complexation, adsorption, competitive precipitation of different salts). The thermodynamic properties of the solutions are usually considered and calculated in the framework of the Debye–Hückel model of ionic solutions: accounting for the increased ionic strength, I, and for the presence of ionic complex-forming agents.

THEORETICAL BACKGROUND

Precipitation, in general, takes place in two stages: nucleation and crystal growth. During the first step, microscopic nuclei of the salt forming are formed from the crystal building blocks, which grow subsequently to macroscopic crystals, which may undergo secondary processes such as aggregation and secondary nucleation. The process may be schematically represented in the block diagram shown in Fig. 1.

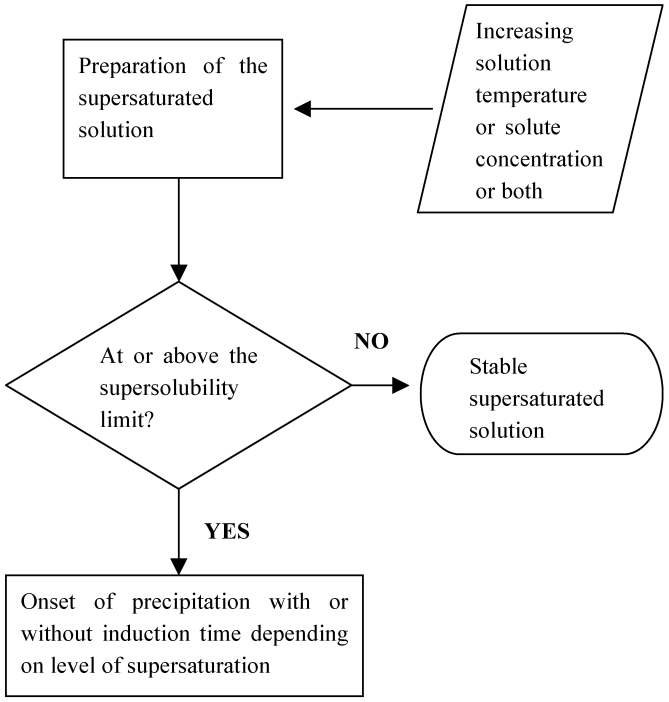

Fig. 1 Block diagram showing the stages involved in the formation of salts from aqueous solutions.

The primary condition necessary for the precipitation process is the establishment of supersaturation, which may be attained by increasing the salt concentration above the equilibrium level. Of primary importance is the development of supersaturation, which is the driving force for nucleation,

and, provided that there is sufficient contact time with a foreign substrate, deposition may take place [1]. Supersaturation is a measure of the deviation of a dissolved salt from its equilibrium value. In Fig. 2, a typical solubility diagram for a sparingly soluble salt of inverse solubility is shown. The solid line corresponds to equilibrium. The conditions of solution composition corresponding to point A correspond to an undersaturated solution. Any deviation from this position may be effected either isothermally (line AC, increasing the solute concentration), at constant solute concentration decreasing the solution temperature (AB), or by varying both concentration and temperature (AD). The points E, F, and G correspond to conditions at which there is equilibrium between the solid phase and the solution, which is saturated with respect to the solute. A solution departing from equilibrium is bound to return to this state by the precipitation of the excess solute. Owing to the presence of secondary minima in the free energy of the solutions, it is possible that the supersaturated solutions formed as described before, may be stable for practically infinite time periods. These solutions are **metastable** and may return to equilibrium only when a cause acts as, for example, the introduction of seed crystals of the salt corresponding to the supersaturated solution.

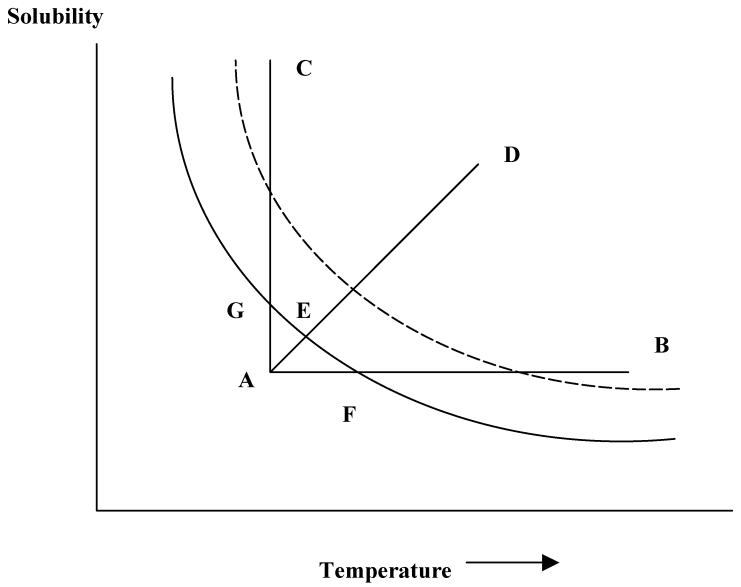

Fig. 2 Solubility isotherm of a salt. Methods of achieving supersaturation: dashed line: supersolubility limit.

There is, however, a threshold in the extent of deviation from equilibrium marked by the dashed line in Fig. 2, which if reached, spontaneous precipitation occurs with or without induction time preceding precipitation. This range of supersaturations defines the **labile** region, and the dashed line is known as the **supersolubility** curve. It should be noted that the supersolubility curve is not well defined and depends on several factors such as presence of foreign suspended particles, agitation, temperature, pH, etc. The formation and subsequent deposition of solids occurs only when the solution conditions correspond to the metastable or the labile region. Below the solubility curve, the corresponding solutions are undersaturated and precipitation cannot take place. On the contrary, the introduction of crystals of the solute in such solutions would result in dissolution.

Supersaturation in solution can be developed in many ways, including temperature fluctuation, pH change, mixing of incompatible waters, increasing the concentration by evaporation, or solids dissolution, etc. Although supersaturation is the driving force for the formation of a salt, the exact values in which precipitation occurs are quite different from salt to salt and as a rule, the degree of super-

saturation needed for a sparingly soluble salt is orders of magnitude higher than the corresponding value for a soluble salt. Quantitatively, supersaturation may be expressed in several types of units [2,3]. Thus, supersaturation is often expressed as concentration difference

$$\Delta C = C - C_{\infty} \tag{1}$$

where C and C_{∞} are the solute concentration in solution and at equilibrium, respectively. The supersaturation ratio (dimensionless), S, is defined as

$$S = \frac{C}{C_{\infty}} \tag{2}$$

$S > 1$ for supersaturated solutions. The relative supersaturation, σ, is defined as

$$\sigma = \frac{C - C_{\infty}}{C_{\infty}} \tag{3}$$

and as may be seen from eqs. 2 and 3

$$\sigma = \frac{C}{C_{\infty}} - 1 = S - 1 \tag{4}$$

For sparingly soluble salts $M_{\nu+}A_{\nu-}$, the supersaturation ratio per ion is defined as

$$S = \left\{ \frac{\left(\alpha_{M^{m+}}\right)_{\mathrm{s}}^{\nu+} \left(\alpha_{A^{\alpha-}}\right)_{\mathrm{s}}^{\nu-}}{\left(\alpha_{M^{m+}}\right)_{\infty}^{\nu+} \left(\alpha_{A^{\alpha-}}\right)_{\infty}^{\nu-}} \right\}^{1/\nu} = \left(\frac{\mathrm{IP}}{K_{\mathrm{s}}^{0}} \right)^{1/\nu} \tag{5}$$

where subscripts s and ∞ refer to solution and equilibrium conditions, respectively, α denotes the activities of the respective ions, and $\nu_+ + \nu_- = \nu$. IP and K_{s}^{0} are the ion products in the supersaturated solution and at equilibrium, respectively. The fundamental driving force for the formation of a salt from a supersaturated solution is the difference in chemical potential of the solute in the supersaturated solution from the respective value at equilibrium

$$\Delta\mu = \mu_{\mathrm{s}} - \mu_{\infty} \tag{6}$$

Since the chemical potential per mole of the solute is expressed in terms of the standard potential and the activity, α, of the solute

$$\Delta\mu = \mu^{0} + RT \ln \alpha \tag{7}$$

where R and T are the gas constant and the absolute temperature, respectively. Substitution of eq. 7 for eq. 6 gives the driving force for solid deposition [4]

$$-\frac{\Delta\mu}{RT} = \ln\left(\frac{\alpha_{\mathrm{s}}}{\alpha_{\infty}}\right) = \ln S \tag{8}$$

For electrolyte solutions, the mean ionic activity is taken

$$\alpha = \alpha_{\pm}^{1/\nu} \text{ where } \nu = \nu_+ + \nu_- \tag{9}$$

and

$$-\frac{\Delta\mu}{RT} = \ln\left(\frac{\alpha_{\pm,s}}{\alpha_{\pm,\infty}}\right)^{\frac{1}{\nu}} = \frac{1}{\nu}\ln S \tag{10}$$

The calculation of the thermodynamic driving force involves the computation of the activities of the component free ions of the salts and consequently of the respective activity coefficients.

The ionic strength of aqueous solutions may reach high values in several cases of practice in which precipitation and/or dissolution takes place. For the computation of the activity coefficients in such media, it is not possible to use the Debye–Hückel expressions, or even extended forms such as the Davies formulation [5]. Semiempirical expressions for the activity coefficients have to be used in these cases [6,7]. The speciation computations may be performed using a number of computer software packages. Most of the software packages available for the speciation computation have been critically reviewed by Nordstom et al. [8]. The calculations proceed iteratively with the minimization of the Gibbs free energy using equilibrium constants for relevant equilibria regardless of mass balance constraints [9].

Nucleation takes place as soon as supersaturation is established. Although there is no general agreement on nucleation, ***primary*** is defined as the nucleation which takes place in the absence of crystalline or any other type of suspended matter. When new crystals are generated in the neighborhood of suspended crystallites or particles, the nucleation is termed ***secondary***. Moreover, the primary nucleation may be further distinguished into homogeneous and heterogeneous to denote situations in which it starts spontaneously or is catalyzed by the presence of foreign particles, respectively. In the primary nucleation, the corresponding rates depend strongly on supersaturation, whereas in secondary nucleation, the size of the crystallites present is reported to be very important [2,3]. According to the classical nucleation theories, the nucleation proceeds through an autocatalytic process of bimolecular reactions resulting in the formation of dimers, trimers, etc. of crystal building blocks, which are the embryos of the crystals to be formed:

$$\begin{gathered}
A + A \leftrightarrows A_2 \\
A_2 + A \leftrightarrows A_3 \\
A_3 + A \leftrightarrows A_4 \\
\cdot \quad \cdot \quad \cdot \\
\cdot \quad \cdot \quad \cdot \\
\cdot \quad \cdot \quad \cdot\cdot \\
A_{n-1} + A \leftrightarrows A_n{}^*
\end{gathered}$$

The cluster $A_n{}^*$ has a critical size that allows for this nucleus to grow further to a macroscopic crystallite. Embryos with size below the critical (subcritical) redissolve.

The nucleation process may be influenced greatly by the presence of impurities in the solutions, which either suppress primary nucleation [4] or promote secondary nucleation [10,11].

Very often, an induction time elapses between the achievement of supersaturation and the detection of the formation of the first crystals. This time, defined as the induction time, τ, is considered to correspond to the time needed for the development of supercritical nuclei. The induction time is inversely proportional to the rate of nucleation, and according to the classical nucleation theory, the following relationship may be written [12]

$$\log\tau = A + \frac{B\gamma_s^3}{(2,303kT)^3 \log S} \tag{11}$$

As soon as stable, supercritical nuclei have been formed in a supersaturated solution, they grow into crystals of visible (at least by physicochemical methods) size. The rate of crystal growth may be

defined as the displacement velocity of a crystal face relative to a fixed point of the crystal. This definition, however, cannot be easily applied to the formation of polycrystalline deposits such as in the case of the formation of calcium phosphates. In this case, the rates of growth may be experimentally expressed in terms of the molar rate deposition by equation

$$R_g = \frac{1}{A}(dm/dt) \tag{12}$$

where m is the number of moles of the solid deposited on a substrate in contact with the supersaturated solution, and A, the surface area of the substrate. Often, linear rates, $\dot{r}$, are used, assuming the shape of the polycrystalline deposits being spherical, of equivalent mean radius, $\bar{r}$

$$\dot{r} = \frac{d\bar{r}}{dt} \tag{13}$$

The molar is related with the linear rate with eq. 14

$$\dot{r} = R_g \frac{M}{\rho} \tag{14}$$

where M is the molecular weight and ρ is the density of the crystalline deposit.

Kinetics and mechanism of crystal growth

The rate laws used to express the dependence of the rates as a function of the solution supersaturation provide mechanistic information for the salt precipitation and/or dissolution mechanism. At a microscopic scale, the sequence of steps followed for the growth of crystals is shown in Fig. 3.

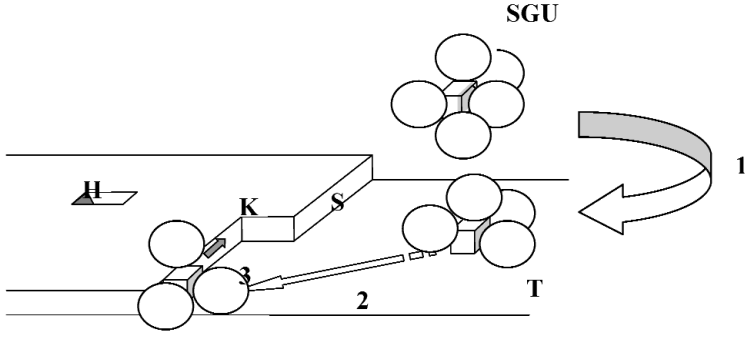

Fig. 3 Schematic outline of the steps involved in the process of crystal growth of the supercritical nuclei.

The steps involved in the crystal growth of the supercritical nuclei are as follows:

i. Transport of the solvated growth units (SGUs) to the surface on crystal terraces (T) by convection or by diffusion (step 1).
ii. Adsorption at a step representing the emergence of a lattice dislocation at the crystal surface accompanied by partial dehydration (step 2).
iii. Migration along the step, integration at a kink site (K) on the step (S), and further dehydration of the growth units (step 3).

The dissolution process may be considered as the reverse of the crystal growth process (detachment of a building block from K, migration along the edge to the step terrace with rehydration, and, finally, migration to the bulk solution).

The rate of crystallization (and of dissolution) can be expressed in terms of the simple semi-empirical kinetics equation

$$R_g = k_g f(S)\sigma^n \tag{15}$$

where k_g is the rate constant for crystal growth, f(S) a function of the total number of the available growth sites, and n the apparent order of the crystal growth process. When mass transport (step 1) is the rate-determining step, the growth rate is given by eq. 16

$$R_d = k_d\sigma \tag{16}$$

where k_d is the diffusion rate constant, given by:

$$k_d = \frac{D\upsilon C_\infty}{\delta} \tag{17}$$

where D is the mean diffusion coefficient of the lattice ions in solution, υ is the molar volume of the crystalline material, C_∞ is the solubility of the precipitating phase, and δ is the thickness of the diffusion layer at the crystal surface [13–16].

From a mechanistic point of view, it is possible to interpret kinetics data on the basis of theoretical models, the most important of which include adsorption and diffusion-reaction. The concept of crystal growth proceeding on the basis of an adsorbed monolayer of solute atoms, molecules, or ion clusters was first suggested by Volmer [17]. Through this monolayer, it is possible to exchange ions or molecules between the bulk solution and the crystal surface. The rate in this case is [18]

$$R_g' = k_{ad}\sigma \tag{18}$$

where the rate constant k_{ad} is given by:

$$k_{ad} = a\nu_{ad}\upsilon C_\infty \tag{19}$$

In eq. 21, a is the jump distance and ν_{ad} the jump frequency of an ion into the adsorption layer.

Since as a rule the growing crystals exhibit the presence of steps on their surfaces, it may be assumed that these steps originate from imperfections or dislocations in the crystal lattice. The uniform deposition of growth units along a step results in the development of spirals which allow for the continuous growth of the crystals since the presence of active sites is maintained. The theory for spiral growth mechanism was developed by Burton, Cabrera, and Frank (BCF theory). According to this theory, the curvature of the spirals near their origin was related to the distance between the successive turns of the spirals and to the solution supersaturation. The growth rate, R_{BCF}, at all supersaturations was given by

$$R_{BCF} = A'\sigma^2 \tanh\left(\frac{B'}{\sigma}\right) \tag{20}$$

where A' and B' are constants that depend on temperature and on the step spacings. At low supersaturations, $\tanh(B'/\sigma) \rightarrow 1$ and $R_{BCF} \propto \sigma^2$, while at high supersaturations, $\tanh(B'/\sigma) \sim B'/\sigma$ and $R_{BCF} \propto \sigma$, i.e., the dependence of the rate of crystal growth on the solution supersaturation changes from a parabolic to a linear dependence as supersaturation increases. It should be noted, however, that although the BCF theory was developed for vapors, it is valid for liquids as well with different expressions for the constants A' and B' [19]. At relatively high supersaturations, it is possible that several two-dimensional nuclei form on the surface of the crystals and spread. In this case, crystal growth can take place

either by the completion of one step at a time (mononuclear mechanism) or by the development of numerous surface nuclei that form steps and kinks in which the incoming ions may be incorporated (polynucleation mechanisms) [20]. The surface nuclei are for the most part of relatively large size, allowing for the development of new nuclei on their surface, i.e., deposition of islands upon islands. In this "birth and spread" model, the rate of crystal growth is

$$R_p = k_p f(s) \exp(-k_p / \ln S) \tag{21}$$

where the polynucleation constant, k_p is

$$k_p = \frac{\pi \gamma_s^2}{3kT^2} \tag{22}$$

In eq. 22, γ_s is the surface energy of the nucleating solid and

$$f(s) = S^{7/6}(S-1)^{2/3}(\ln S)^{1/6} \tag{23}$$

Spiral and polynuclear control in the mineral scale formation are parallel, with the faster controlling the overall mechanism. However, mass transport to the crystal surface, adsorption of lattice ions, and the mechanisms at the crystal surface are consecutive steps, and the slowest is the rate-determining step. Knowledge for the operative mechanism may be obtained by fitting experimental data into eq. 15. Supportive evidence can also be obtained by the investigation of the role of fluid dynamics on the rates of crystal growth. Dependence of the growth measured on the fluid velocity suggests mass transport control for the rates of deposition.

EXPERIMENTAL METHODOLOGY

Crystal growth and dissolution processes may be investigated from supersaturated solutions prepared directly in double-walled, water-jacketed glass reactors in order to control temperature accurately. This parameter is important for the solubility and speciation of the system in which nucleation is studied. At rather high supersaturations in the calcium phosphate system, past the lapse of induction times, solution opalescence appears, which is associated with the formation of a solid phase. The spontaneous precipitation is associated with a decrease of the solution pH. The process may be investigated either by monitoring the solution pH or by sampling and following the desupersaturation through chemical analysis of the liquid phase for calcium and phosphorus in solution. Alternatively, the process may be investigated at constant pH using an automatic titrator and recording the volume of alkali consumed to keep the solution pH constant with time. Precipitation in relatively high supersaturated calcium phosphate solutions results in the formation of intermediate calcium phosphate phases which are converted by an autocatalytic hydrolysis process to the thermodynamically most stable hydroxyapatite [$Ca_5(PO_4)_3OH$, HAP]. More specifically, at very high supersaturations, the unstable amorphous calcium phosphate precursor is formed [21–23]. Other precursor phases forming past the appearance of the first solid include octacalcium phosphate [$Ca_8H_2(PO_4)_6 \cdot 5H_2O$, OCP] [24,25] and dicalcium phosphate dihydrate [$CaHPO_4 \cdot 2H_2O$, DCPD] [26]. The lifetime of the various intermediate phases varies depending on the solution supersaturation. Fast conversions take place at lower supersaturations as a rule [27]. As a result, these studies often suffer from the difficulty of providing reliable kinetics data concerning the mineral phase forming. The rates of precipitation measured when transient phases form are rather unreliable and hard to reproduce. Moreover, small analytical errors in the analysis of calcium and phosphorus in the precipitating solids introduce large uncertainties concerning the nature of the precipitating solid. On the other hand, at very high supersaturation, the induction times measured are not reproducible. Alternatively and in order to overcome problems associated with spontaneous precipitation, seeded

techniques, limited to lower supersaturations, were developed [28]. According to this methodology, stable supersaturated solutions are directly prepared in a reactor, the temperature of which is controlled through an external thermostat. Following confirmation of the stability of the solutions carefully measured, a well-characterized amount of seed crystals of the salt under investigation is suspended. Crystal growth may proceed either instantaneously or past the lapse of induction times [29]. The crystallization process, as in the case of spontaneous precipitation, may be monitored either at constant pH (pH-stat method) or at variable pH (free-drift method). In either case, additional monitoring of the solution supersaturation is needed by sampling of the suspensions filtering and analysis of the filtrates for calcium and phosphorus. From the profiles of the calcium or phosphorus vs. time, the rates of precipitation may be determined by polynomial fit of the data [30]. Despite the fact that this methodology provided for high reproducibility, the problem of confusing crystal phases transforming rapidly at lower or decreasing supersaturations was not overcome. On the other hand, experiments done at very low supersaturations were of high uncertainty as the changes of the lattice ions concentrations in the solutions were too small to provide reliable concentration–time profiles for the measurement of the kinetics.

All problems related to both the spontaneous precipitation and the seeded growth techniques were overcome with the employment of the constant supersaturation technique, which has been applied over a wide range of sparingly soluble salts from calcium phosphates [31,32]. Magnesium ammonium phosphate hexahydrate or struvite [33,34] calcium carbonate [35], etc. The concept of the methodology is to replace in solution the ions that are removed by precipitation. The prerequisite for the application of this methodology is the possibility of monitoring the crystal growth process through the measurement of a solution parameter using a sufficiently sensitive sensor. In the case of the phosphate salts, including calcium phosphates and magnesium ammonium phosphate, for example, the precipitation is accompanied with proton release. A glass/reference pair of electrodes may be used to monitor the precipitation process of this type of salts. The sensor signal may provide feedback to an electronic arrangement that activates a system of pumps which add titrant solutions with the appropriate composition added to the supersaturated solutions so that the activities of all ions are kept constant. This concept may well be applied to the dissolution of salts. Examples for the titrant composition for the crystal growth of struvite ($MgNH_4PO_4 \cdot 6H_2O$) and for the dissolution of calcium carbonate are given below.

Crystal growth of struvite at constant supersaturation [34]

Assuming that the aqueous solution contains solutions of concentrations: x_1 M $MgSO_4 \cdot 7H_2O$, x_2 M $NH_4H_2PO_4$, x_3 M NaOH, and x_4 M synthetic wastewater (SWW), the titrant solution should contain y_1 M $MgSO_4 \cdot 7H_2O$, y_2 M $NH_4H_2PO_4$, y_3 M NaOH, and y_4 SWW in order to maintain the activities of all ions constant. Assuming dm moles of $MgNH_4PO_4$ precipitated, in the total volume of the supersaturated solution, V, and dV the respective titrant solution volume added by each burette, the requirement for constant magnesium activity imposes the mass balance eq. 2, from which the concentration of magnesium in the titrant, y_1, is obtained:

$$x_1 = \frac{x_1 \cdot V + y_1 \cdot \mathrm{d}V - \mathrm{d}m}{V + 2\mathrm{d}V} \Rightarrow 2x_1 = y_1 - \frac{\mathrm{d}m}{\mathrm{d}V} \Rightarrow y_1 = 2x_1 + c \tag{24}$$

where $\mathrm{d}m/\mathrm{d}V = c$ is a measure of the amount of solid precipitated per unit volume. This parameter was determined empirically, by preliminary experiments.

Similarly, the requirement of titrant solution addition for constant phosphate activity is

$$y_2 = 2x_2 + c \tag{25}$$

Owing to the fact that two protons are released to the solution during the precipitation of each mole of solid, sodium hydroxide titrant is needed with a concentration y_3

$$y_3 = 2x_3 + 2c \tag{26}$$

Similarly, the requirement for the SWW is

$$y_4 = 2x_4 - 2c \tag{27}$$

The titrant solutions were, therefore, prepared as follows:

Titrant 1: $(2x_1 + c)$M $MgSO_4 \cdot 7H_2O$ + $(2x_4 - 2c)$M background electrolyte
Titrant 2: $(2x_2 + c)$M $NH_4H_2PO_4$ + $(2x_3 - 2c)$M NaOH + $(2x_4 - 2c)$M background electrolyte

In our experiments, the value of $c = 20$, was obtained from preliminary experiments in which it was found adequate to keep the solution supersaturation constant. The time lapsed between the preparation of the supersaturated solutions (including pH adjustment) and the first addition of the titrant solution was taken as the induction time, τ.

Dissolution of calcium carbonate at constant undersaturation [35]

Assuming that the working solution, volume totalling V, consists of x_1 M $CaCl_2$, x_2 M $NaHCO_3$, x_3 M NaOH (for the pH adjustment), and x_4 M NaCl (for the ionic strength adjustment), the titrant solutions should contain y_1 M $CaCl_2$, y_2 M $NaHCO_3$, y_3 M HCl, and y_4 M NaCl, in order to maintain supersaturation during the course of dissolution. If the volume added by each burette is dV, for constant calcium concentration, the mass balance requires that

$$\chi_1 = \frac{\chi_1 V + y_1 \mathrm{d}V + \mathrm{d}m}{V + 2\mathrm{d}V} \tag{28}$$

where dm are the moles of calcium released from the dissolution of calcium carbonate. From eq. 28, the concentration of $CaCl_2$ in the titrant solution 1 should be

$$y_1 = 2\chi_1 - \frac{\mathrm{d}m}{\mathrm{d}V} \tag{29}$$

The ratio $\mathrm{d}m/\mathrm{d}V \equiv c$, is called the effective dissolution constant, a measure of the amount of solid released by dissolution per unit volume and is determined by preliminary experiments. Similarly, for constant carbonate concentration in solution, it should be

$$y_2 = 2x_2 - c \tag{30}$$

Assuming that two proton equivalents are withdrawn per mole of $CaCO_3$ dissolved. The HCl concentration in the titrants is

$$y_3 = 2(-x_3) + 2c \tag{31}$$

The minus sign corresponds to the fact that, for the working solution pH adjustment to the value 8.25, NaOH addition is needed while HCl is needed for balancing hydroxyl release during dissolution. Finally, the inert electrolyte content of the titrants is

$$y_4 = 2x_4 - c \tag{32}$$

The titrant solutions in the two burettes were as follows:

Titrant 1: $y_1 + y_3$
Titrant 2: $y_2 + y_4$

The restriction for the value of c is $c \le 2x_1, 2x_2$.

The main advantages of the methods to study crystal growth and dissolution processes at constant solution composition are, besides the high accuracy and reproducibility, the possibility of carrying out

experiments very close to the solubility isotherm, i.e., at very low degrees of super- or undersaturation. At these conditions, all other methods fail owing to the very small changes in the solute concentrations, which do not allow the identification of the precipitating mineral salts. Of particular interest is the application of the constant supersaturation in the investigation of heterogeneous nucleation (e.g., the formation of calcium phosphate on biomaterials) or in studies of crystal growth in the presence of additives which may adsorb on the crystals often used to seed the supersaturated solutions.

RESULTS AND DISCUSSION

Calcium phosphate system: Biological mineralization

Body fluids are supersaturated with respect to calcium phosphates. The calcium phosphate system is rather complicated because it is possible that a number of solids may precipitate out. The possible phases that may be formed in supersaturated solutions are summarized in Table 1.

Table 1 Calcium phosphates and the respective solubility products [37].

Name of solid	Formula	Abbreviation	Solubility product
Dicalcium phosphate dihydrate	$CaHPO_4 \cdot 2H_2O$	DCPD	1.87×10^{-7} (mol $L^{-1})^2$
Dicalcium phosphate anhydrous	$CaHPO_4$	DCPA	9.2×10^{-8} (mol $L^{-1})^2$
β.Tricalcium phosphate	$Ca_3(PO_4)_2$	TCP	2.8×10^{-9} (mol $L^{-1})^{15}$
Octacalcium phosphate	$Ca_8H_2(PO_4)_6 \cdot 5H_2O$	OCP	2.5×10^{-99} (mol $L^{-1})^{16}$
Hydroxylapatite	$Ca_{10}(PO_4)_6(OH)_2$	HAP	5.5×10^{-118} (mol $L^{-1})^{18}$

In vitro studies of biological calcification may be done in an acellular simulated body fluid (SBF) with ion concentrations nearly equal to those of the human blood plasma [38]. The problem often is that the use of SBF in mineralization studies sometimes may yield doubtful results because the supersaturations involved are relatively high and, on the other hand, the pH constancy is ensured by the use of buffer solutions (tris-buffer) that contain organic compounds which may interfere with the nucleation and crystal growth processes. The realization of deviation from physiological conditions have prompted studies using modified SBF [39,40]. In our studies, we have used the constant composition approach to investigate mineralization of porcine heart valves using SBF solutions in which we could vary the supersaturation. The composition of the SBF solutions used is summarized in Table 2.

Table 2 Composition of the SBF used in mineralization experiments at constant supersaturation.

Ion	Working solution 10^{-3} M	Human plasma 10^{-3} M
Na^+	142.0	142.0
K^+	5.0	5.0
Ca^{2+}	in the range 1.5–3.3	2.5
Mg^{2+}	1.5	1.5
HCO_3^-	4.2	27.0
Cl^-	148.0	103.0
HPO_4^{2-}	1.0	1.0
SO_4^{2-}	0.5	0.5

The substrates on which the mineralization process was tested consisted of porcine heart valves, fixed with glutaraldehyde. The experimental set-up is outlined in Fig. 4.

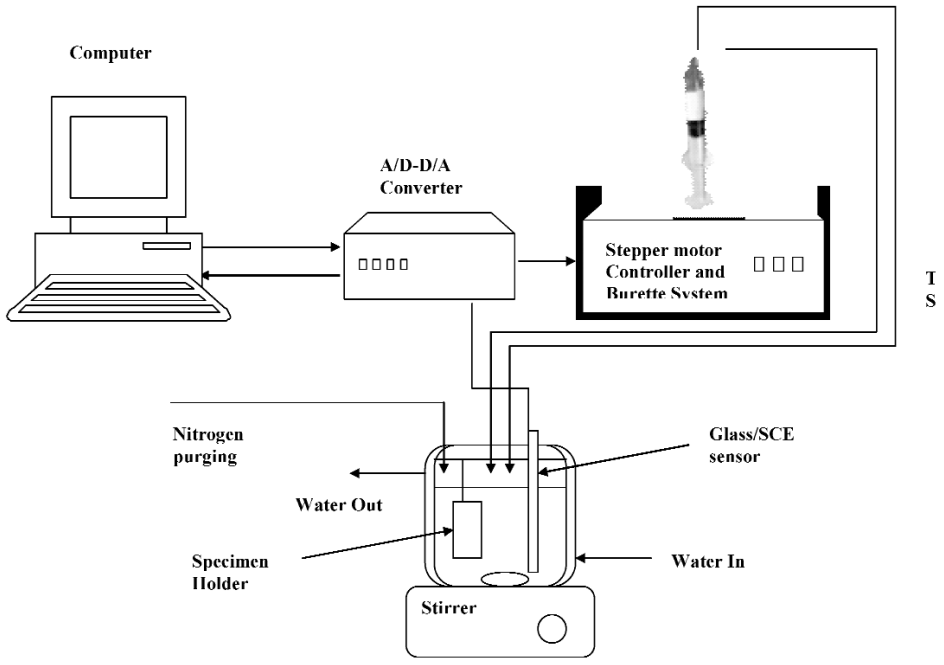

Fig. 4 Experimental set-up for the mineralization experiments.

The valve material substrates were fixed in special Perspex frames so as to expose the maximum possible surface area in the supersaturated solutions. The layout of the reactor with the mounted valves is shown schematically in Fig. 5.

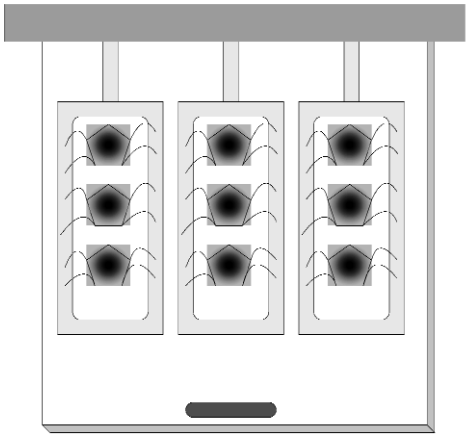

Fig. 5 Schematic of the reactor and the mounted heart valves.

Using the constant supersaturation methodology, the pH of the solution and the activities of all ions were kept constant while from the rate of addition of the titrants solutions it was possible to cal-

culate the rates of formation of the calcium phosphate on the heart valve tissues. The results obtained from a typical experiment are shown in Figs. 6 and 7, where the constant solution pH and the rate of titrants addition are shown, respectively.

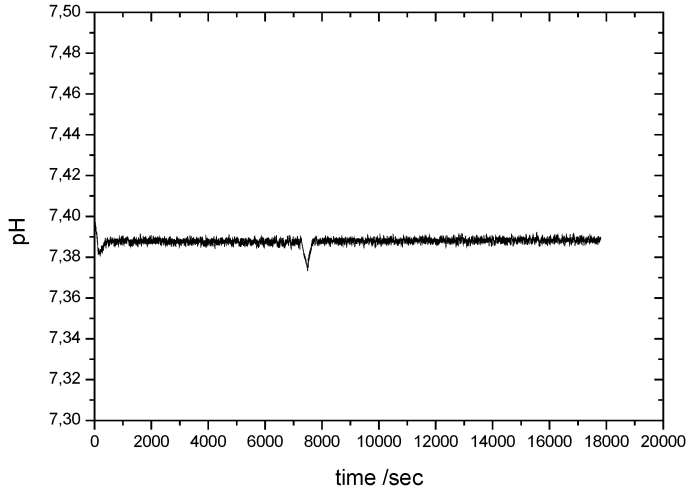

Fig. 6 Solution pH during the course of deposition of calcium phosphate on porcine heart valves treated with glutaraldehyde. 37 °C, σ_{HAP} = 12.15, SBF.

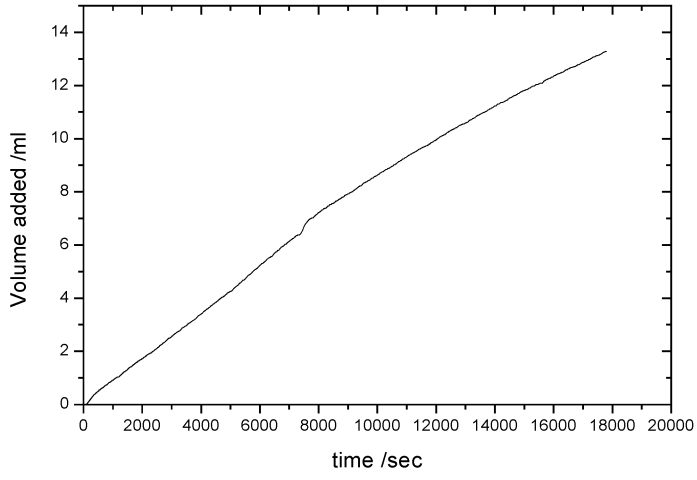

Fig. 7 Titrants addition during the course of deposition of calcium phosphate on porcine heart valves treated with glutaraldehyde. 37 °C, σ_{HAP} = 12.15, SBF.

The presence of the substrate was the catalyst for the nucleation of calcium phosphate. The type of the precipitating calcium phosphate salt was determined by the solution supersaturation. At solution supersaturations just over the solubility isotherm of OCP, it was found that this phase was stabilized. Typical plate-like formations of OCP crystallites grown on the collagenous side of the heart valve leaflets are shown in Fig. 8.

In all cases, the rates measured were found to depend on the solution supersaturation showing a parabolic dependence suggesting that the process is surface diffusion-controlled.

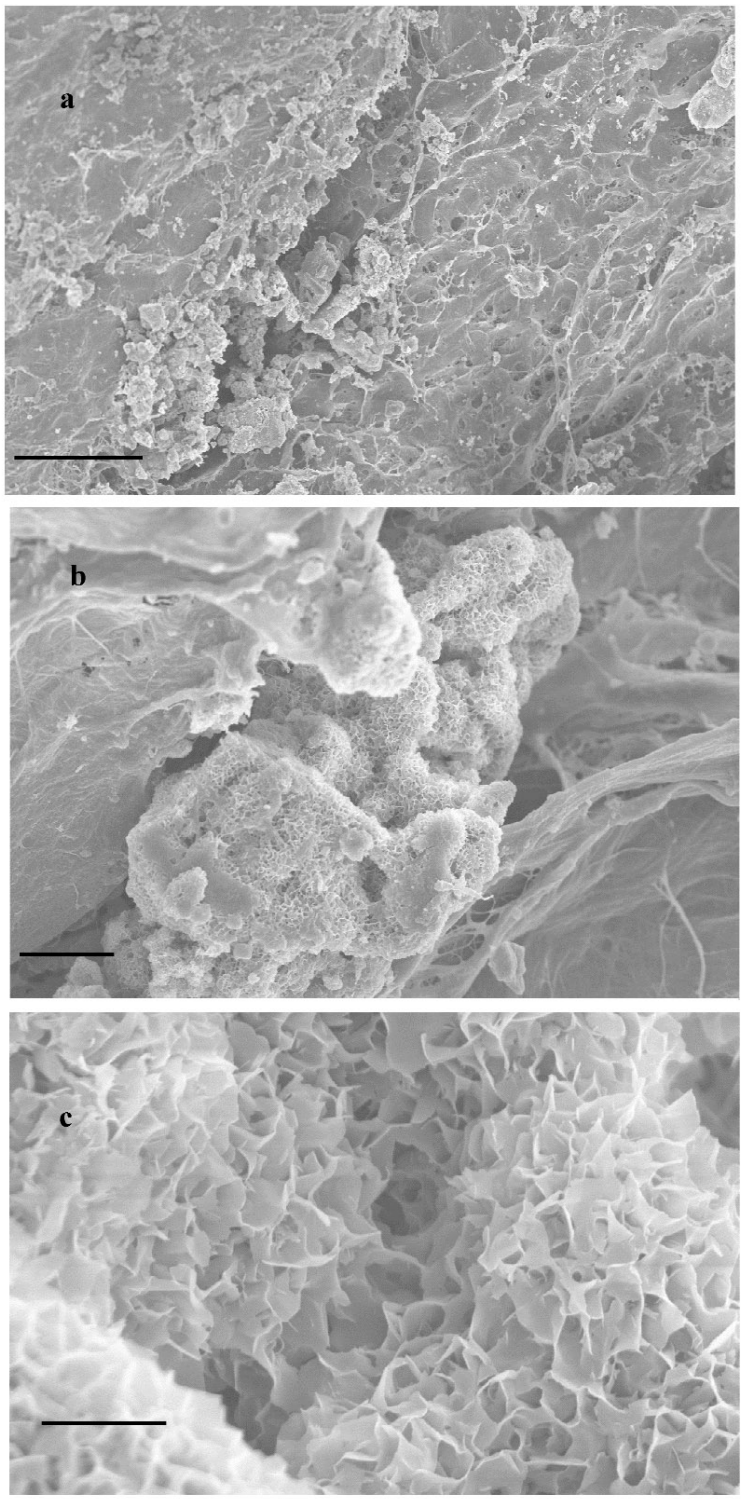

Fig. 8 Deposition of calcium phosphate on porcine heart valves treated with glutaraldehyde; pH 7.40, 37 °C, total calcium 1.0 mM, total phosphate 0.6 mM in SBF (a: bar 100 μm, b: 10 μm, c: 2 μm).

Magnesium ammonium phosphate hexahydrate (struvite) system

The formation of struvite was investigated in SWW with the composition shown in Table 3. Solution supersaturation was achieved by rapid mixing of SWW and $NH_4H_2PO_4$. Next, the pH was adjusted at 8.50 or 9.00 by the addition of appropriate amount of NaOH 1 M, followed by the addition of the Mg stock solution. Finally, the pH was adjusted again at 8.50 or 9.00. The experiments were done at least in triplicate for the assessment of repeatability. According to the precipitation reaction

$$Mg^{2+} + NH_4^+ + H_2PO_4^- \Leftrightarrow MgNH_4(PO_4)_3{\cdot}6H_2O + 2H^+$$

protons released into the solution during the precipitation of struvite. Moreover, a drop of pH higher than 0.005 pH units triggered the addition of standard NaOH solution from the burette of a computerized automatic titrator.

Table 3 Chemical composition of SWW solution for experiments at constant supersaturation.

Component	Concentration
Glucose	0.517 mM (equal to 100 ppm chemical oxygen demand, COD)
$NaHCO_3$	17.86 mM
NaCl	10 mM
$NaNO_3$	0.5882 mM
Na_2SO_4	15 mM

The titrant solutions were made as follows by the stock solutions of magnesium and phosphate, the SWW solution, and the NaOH solution:

Titrant 1: $(2x_1 + c)$ M $MgSO_4{\cdot}7H_2O$ + $(2x_4 - 2c)$ M SWW
Titrant 2: $(2x_2 + c)$ M $NH_4H_2PO_4$ + $(2x_3 - 2c)$ M NaOH + $(2x_4 - 2c)$ M SWW

where x_1, x_2, x_3, and x_4 are the concentrations of the salts indicated and c is an arbitrary constant. In our experiments, $c = 20$, this value was determined from preliminary experiments in order to keep the solution supersaturation constant. The equilibria considered for the system of the SWW, in which the solution supersaturation was adjusted with the addition of the appropriate concentrations of magnesium sulfate and ammonium phosphate, are summarized in Table 4. The induction times measured before the onset of spontaneous precipitation in the supersaturated solutions were inversely proportional to the solution supersaturation with respect to struvite, as seen in Fig. 9.

As seen in Fig. 9, the supersaturation domain in which the corresponding solutions are stable over very long time periods (time periods as long as 24 h were taken as defining the limits of the "stable" metastable zone) with respect to struvite precipitation, is rather narrow. Moreover, the presence of the additional ions in the SWW changed the stability diagram of the system, favoring destabilization of the system at lower solution supersaturation in comparison with the system in the presence of sodium chloride alone. These results, however, indicate it is possible that they reflect changes in the solubility of struvite in SWW.

Table 4 Equilibrium involved in the computation of the solution speciation (I = 0, 25 °C) when $MgSO_4 \cdot 7H_2O$ stock solution was used. Values from ref. [37].

Equilibria	log k	Equilibria	log k
$H^+ + PO_4^{3-} \Leftrightarrow HPO_4^{2-}$	12.375	$Mg^{+2} + CO_3^{2-} \Leftrightarrow MgCO_3$	2.92
$H^+ + HPO_4^{2-} \Leftrightarrow H_2PO_4^-$	7.198	$Mg^{+2} + HCO_3^- \Leftrightarrow MgHCO_3^+$	1.01
$H^+ + H_2PO_4^- \Leftrightarrow H_3PO_4$	2.148	$NH_3 + H^+ \Leftrightarrow NH_4^+$	9.244
$Na^+ + PO_4^{3-} \Leftrightarrow NaPO_4^{2-}$	1.43	$NH_3 + Mg^{+2} \Leftrightarrow MgNH_3^{+2}$	0.24
$Na^+ + HPO_4^{2-} \Leftrightarrow NaHPO_4^-$	1.07	$2NH_3 + Mg^{+2} \Leftrightarrow Mg(NH_3)_2^{+2}$	0.2
$Na^+ + H_2PO_4^- \Leftrightarrow NaH_2PO_4$	0.3	$3NH_3 + Mg^{+2} \Leftrightarrow Mg(NH_3)_3^{+2}$	–0.3 (I = 2)
$Na^+ + NaPO_4^{2-} \Leftrightarrow Na_2PO_4^-$	1.16	$H^+ + SO_4^{2-} \Leftrightarrow HSO_4^-$	1.99
$H^+ + Na_2PO_4^- \Leftrightarrow Na_2HPO_4$	10.73	$Na^+ + SO_4^{2-} \Leftrightarrow NaSO_4^-$	0.73
$Mg^{+2} + PO_4^{3-} \Leftrightarrow MgPO_4^-$	4.8	$NH_4^+ + SO_4^{2-} \Leftrightarrow NH_4SO_4^-$	1.03
$Mg^{+2} + HPO_4^{2-} \Leftrightarrow MgHPO_4^-$	2.80	$Mg^{+2} + SO_4^{2-} \Leftrightarrow MgSO_4$	2.26
$Mg^{+2} + H_2PO_4^- \Leftrightarrow MgH_2PO_4$	0.45	$H^+ + OH^- \Leftrightarrow H_2O$	13.997
$Na^+ + NO_3^- \Leftrightarrow NaNO_3$	–0.55	$Na^+ + OH^- \Leftrightarrow NaOH$	0.1
$H^+ + CO_3^{2-} \Leftrightarrow HCO_3^-$	10.329	$Mg^{+2} + OH^- \Leftrightarrow MgOH^+$	2.6
$H^+ + HCO_3^- \Leftrightarrow H_2CO_3$	6.352	$Na^+ + Cl^- \Leftrightarrow NaCl$	–0.5
$H_2O + CO_2 \Leftrightarrow H_2CO_3$	–1.466	$Mg^{+2} + Cl^- \Leftrightarrow MgCl^+$	0.6
$Na^+ + CO_3^{2-} \Leftrightarrow NaCO_3^-$	1.27	$Mg^{+2} + PO_4^{-3} + NH_4 + 6 \cdot H_2O \Leftrightarrow$	13.26
$Na^+ + HCO_3^- \Leftrightarrow NaHCO_3$	–0.25	$MgNH_4(PO_4)_3 \cdot 6H_2O$	

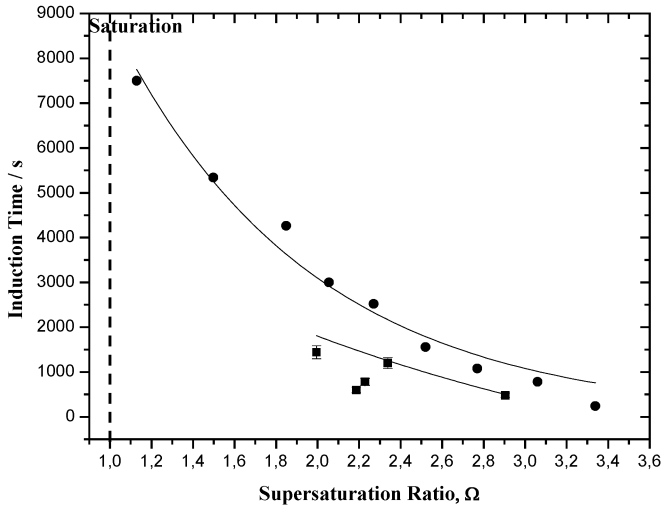

Fig. 9 Stability diagrams for the precipitation of struvite at 25 °C, pH 8.50; (●) 0.15 M NaCl; (■): SWW.

The kinetics of spontaneous formation of struvite in SWW showed parabolic dependence, as seen in Fig. 10.

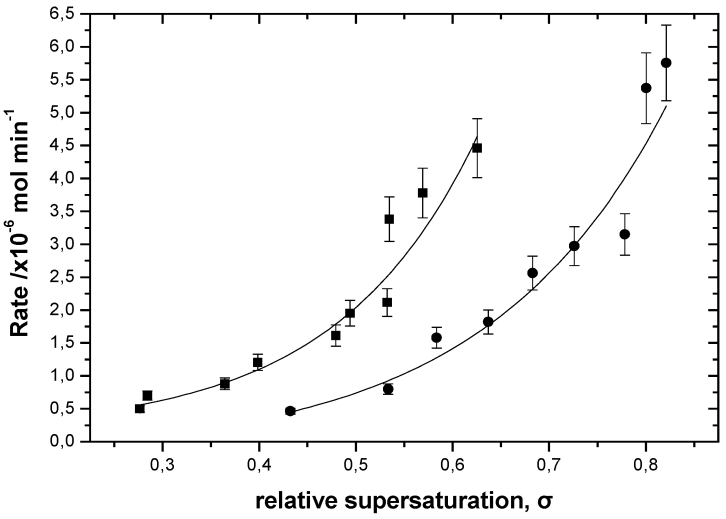

Fig. 10 Kinetics of spontaneous precipitation of struvite for different pH values; 25 °C, pH 8.50 (■); pH 8.0 (●).

The morphology of the precipitated crystals in SWW did not vary significantly, and it was the same with the corresponding habit in the absence of foreign ions. Changes in the crystal habit were observed at higher pH. At pH 9.50, the crystals formed showed a plate-like habit. It should also be noted that in the presence of additives, which retarded the crystal growth rates, the crystals formed were larger in comparison with the crystals grown without inhibition. Typical morphology of the struvite crystals is shown in Fig. 11.

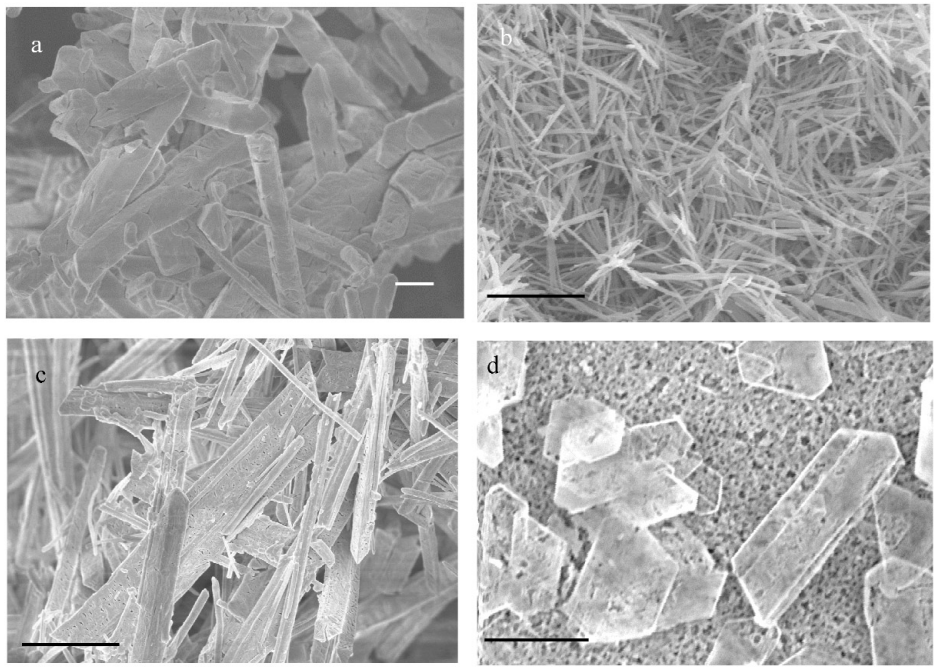

Fig. 11 Struvite crystals precipitated from solution at conditions of constant solution composition; a: pH 7.00 (bar 2 μm), b: pH 8.00 (bar 15 μm); c: pH 9.0 (bar 10 μm); pH 9.50 (bar 10 μm).

The evaluation of the rates of precipitation and/or dissolution of struvite necessitates knowledge of the solubility of the respective solid. A series of measurements was done over a wide range of ionic strength values. The solubility was measured both from super- and undersaturated solutions. The solutions, following their preparation in Erlenmeyer flasks, were seeded, sealed with rubber stoppers, and placed in a thermostatted bath to keep temperature constant (25 °C) and were stirred frequently to ensure homogeneity. Samples were withdrawn at various time intervals and over a time period of two years. Immediately following the opening of the flasks, pH was measured and the withdrawn samples were next filtered and the filtrate was analyzed for magnesium and phosphate. The flasks were re-sealed and placed again in the thermostat. The initial conditions are summarized in Table 5.

Table 5 Super- and undersaturated with respect to struvite solutions for the measurement of struvite solubility.

	Precipitation				Dissolution			
Ionic strength/M	0.2	0.15	0.1	0.05	0.2	0.15	0.1	0.05
$MgCl_2 \cdot 6H_2O$ (M)	1×10^{-2}	1×10^{-2}	1×10^{-2}	1×10^{-2}	1×10^{-3}	1×10^{-3}	1×10^{-3}	1×10^{-3}
$NH_4H_2PO_4$ (M)	1×10^{-2}	1×10^{-2}	1×10^{-2}	1×10^{-2}	1×10^{-3}	1×10^{-3}	1×10^{-3}	1×10^{-3}
NaCl (M)	0.165	0.115	0.065	0.015	0.1965	0.1465	0.0965	0.0465
Ω	1.840	2.100	2.490	3.080	0.003	0.003	0.004	0.006
$m_{struvite}$ (mg) suspended	50	50	50	50	50	50	50	50

The ion activity product (IAP) of struvite is:

$$\begin{aligned}(\mathrm{IAP}) &= \left(\mathrm{Mg^{2+}}\right)\left(\mathrm{NH_4^+}\right)\left(\mathrm{PO_4^{3-}}\right) = \left[\mathrm{Mg^{2+}}\right]\cdot\gamma_2\cdot\left[\mathrm{NH_4^+}\right]\cdot\gamma_1\cdot\left[\mathrm{PO_4^{3-}}\right]\cdot\gamma_3 \Rightarrow \\ (\mathrm{IAP}) &= \left[\mathrm{Mg^{2+}}\right]\cdot\gamma_1^4\cdot\left[\mathrm{NH_4^+}\right]\cdot\gamma_1^1\cdot\left[\mathrm{PO_4^{3-}}\right]\cdot\gamma_1^9 = (\mathrm{ICP})\cdot\gamma_1^4\cdot\gamma_1^1\cdot\gamma_1^9\end{aligned} \tag{33}$$

or

$$(\mathrm{IAP}) = (I.C.P)\cdot\gamma_1^{14} \tag{34}$$

Substitution of the activity coefficient with the Davies expression [10], yields

$$\log(I.C.P) = \log(\mathrm{IAP}) + 14A\left(\frac{\sqrt{I}}{1+\sqrt{I}} - 0.3I\right) \tag{35}$$

Plots of log(*I.C.P.*) as a function of $\left(\frac{\sqrt{I}}{1+\sqrt{I}} - 0.3I\right)$ are expected to yield straight lines. Extrapolation to ionic strength 0, yields the value of the thermodynamic solubility product:

$$K_{sp}^0 = (\mathrm{IAP})_{I\to 0} \tag{36}$$

In Fig. 12, the plot according to eq. 35, may be seen.

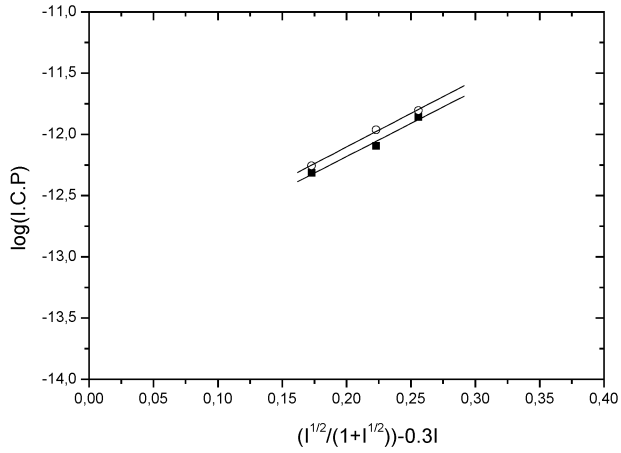

Fig. 12 Plot of the logarithm of the ion concentration product (ICP) as a function of the logarithm of the Davies expression for the activity coefficients. (○): data from precipitation; (■): data from dissolution. Equilibration time: 65 days, 25 °C.

It was found that 60 days was sufficient time to reach equilibration. Measurements were identical up to 800 days. The differences between the lines obtained from precipitation and dissolution were within the experimental error. Extrapolation to zero ionic strength yielded for the thermodynamic solubility product the value of

$$\log K_{\mathrm{sp}}^{0} = \log(\mathrm{IAP})_{I\to 0} = -13.68 \pm 0.26$$

The approach to equilibrium is shown in Fig. 13 in which the IAP calculated from the samples collected at various time intervals is plotted as a function of time.

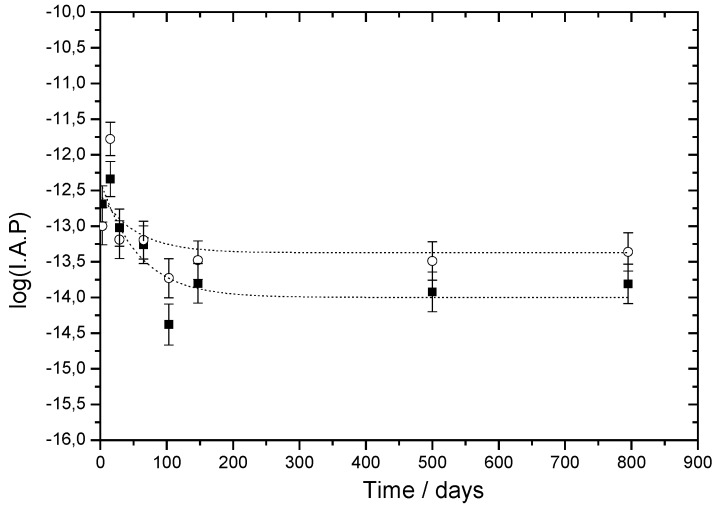

Fig. 13 Logarithm of the IAP of struvite calculated at various time intervals from solutions approaching equilibrium from: (○): dissolution; (■): precipitation, at 25 °C.

The interaction of the precipitated crystallites in the supersaturated solutions with foreign ions, compounds, and/or macromolecules depends strongly on the surface charge of the solids, which depends on the concentration of the potential-determining ions, i.e., the lattice ions of struvite [41]. The variation of the ζ-potential as a function of the solution concentration of the potential-determining ions in sodium chloride and in SWW media is shown in Figs. 14 and 15, respectively. As may be seen, the isoelectric point in 0.1 M NaCl was determined at $pMg \approx pNH_4^+ \approx 1.2$. Increasing phosphate ion concentration in solution resulted in higher negative electric charge. In SWW, the surface charge of the struvite particles remained negative and showed relatively little change with the variation of the concentration of the potential-determining ions over a wide range of concentrations of the potential-determining ions. In terms of surface charge variation, as may be seen in Fig. 15, it was only the concentration of the magnesium ions which showed the most pronounced effect.

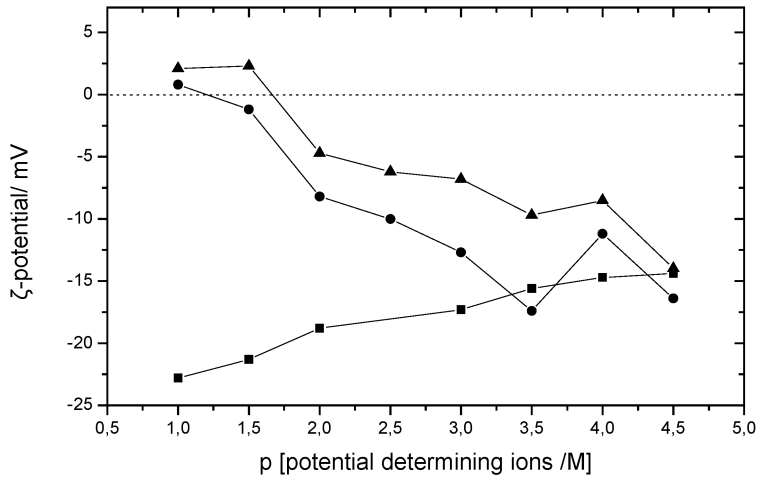

Fig. 14 ζ-potential variation as a function of the concentration of the potential determining ions in 0.1 M NaCl; (▲): ammonium ions; (■): phosphate ions; (●): magnesium ions; 25 °C. Dotted line indicates isoelectric point.

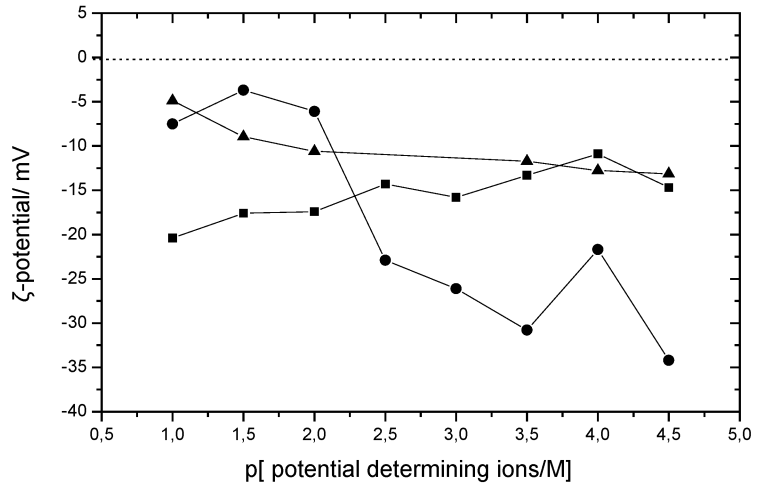

Fig. 15 ζ-potential variation as a function of the concentration of the potential determining ions in SWW; (▲): ammonium ions; (■): phosphate ions; (●): magnesium ions; 25 °C. Dotted line indicates isoelectric point.

Dissolution of sparingly soluble salts

The dissolution of a sparingly soluble salt, from the mechanism point of view, may be looked upon as the mirror image of the crystallization process. The investigation of the dissolution process takes place from undersaturated solutions, following the dispersion of the corresponding salt. As in the case of crystal growth, the degree of the solution undersaturation determines the rate of dissolution of a sparingly soluble salt. Dissolution of calcium carbonate, a major component of building materials, is considered to be among the major causes of deterioration of monuments and artifacts exposed in environmental conditions. Thus, in an acid rain environment, dissolution is fast and destructive [42–45]. An alkaline environment, often developed when incompatible materials are brought together in conservation ventures (e.g., using Portland cement to repair marble fractures) may also be aggressive and destructive, promoting dissolution of the calcitic material [46]. The dissolution of a calcitic solid, Carrara marble, shall be presented next. Carrara marble is a material which has been widely used for the construction of monuments of the European cultural heritage. The material has been well characterized and was used in dissolution experiments in a powdered form [47]. The dissolution of calcium carbonate in aqueous media may be described by the following equations [48]:

$$H^+ + CaCO_3 \leftrightarrows Ca^{2+} + HCO_3^- \quad \text{(i)}$$

$$H_2CO_3 + CaCO_3 \leftrightarrows Ca^{2+} + 2HCO_3^- \quad \text{(ii)}$$

$$H_2O + CaCO_3 \leftrightarrows Ca^{2+} + HCO_3^- + OH^- \quad \text{(iii)}$$

Reaction iii dominates the dissolution process at the experimental pH. The rates of dissolution were calculated from the time profiles of the titrant solutions addition. The rates of dissolution decreased as a function of time, despite the fact that the solution undersaturation was kept constant by the addition of titrant solutions [49]. The decrease in the rates of dissolution of the seed crystals inoculating the undersaturated solutions was attributed either to the elimination of the active sites or to the participation of critical conditions involving dissolution steps. The extent of dissolution, α, was in all cases calculated from the volume of the titrants added, V:

$$\alpha = \frac{m_{\text{diss}}}{m_{\text{o}}} \times 100 = \frac{C_{\text{HCl}} \cdot FW_{\text{CaCO}_3} \cdot V_{\text{HCl}}}{m_0} \times 100 \quad (37)$$

where m_{diss} and m_{o} are the dissolved and initial mass of marble powder respectively, C_{HCl} the concentration (M) of hydrochloric acid used in the titrants, and V_{HCl} the respective volume of the acid added [36]. The driving force for dissolution at constant temperature depends on the solution undersaturation, Ω:

$$\Omega = \frac{\left(Ca^{2+}\right) \cdot \left(CO_3^{2-}\right)}{K_{\text{s}}^0} = \frac{\text{IP}}{K_{\text{s}}^0} \quad (38)$$

where IP is the ion product for calcite in the undersaturated solutions and K_{s}^0 is the respective thermodynamic solubility product. The relative solution undersaturation, σ, taking into account mean ion activities is

$$\sigma = 1 - \Omega^{\frac{1}{2}} \quad (39)$$

The relationship between the rates of dissolution and the solution undersaturation, which may yield mechanistic information, necessitates knowledge of the value of the thermodynamic solubility product for the material investigated. The thermodynamic solubility product of the Carrara powdered

marble was measured by equilibration of the solid in solutions of sodium chloride at three different concentration values. The solutions were sealed and thermostatted at 25 °C. The suspensions of the marble powder were thoroughly mixed, and samples were withdrawn periodically and up to a time period of two years. The solution pH and calcium concentration was monitored by measurements in the suspensions with a glass/silver-silver chloride combination electrode, sampling, filtration, and analysis of the filtrates. For Carrara marble and past an equilibration time of two years, the value of 7.77 ± 0.05 was estimated for the thermodynamic solubility product by extrapolation to zero ionic strength. The calculated solubility isotherms for synthetic calcite and for the calcitic Carrara marble are shown in Fig. 16.

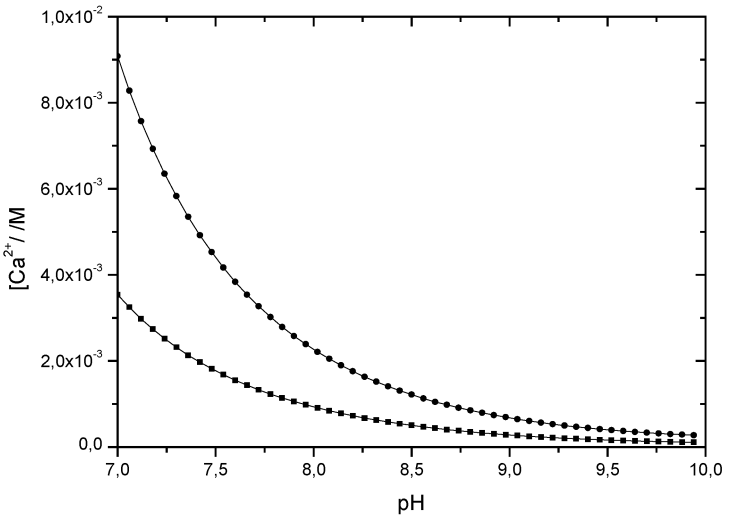

Fig. 16 Solubility isotherms: (●): Carrara marble; (■): synthetic calcite, 25 °C.

It may be seen from the isotherms that the Carrara marble is more soluble than calcite. This may be due to the structure of the solid and/or to the content of metallic impurities which may enter the calcitic lattice. The conditions of the dissolution experiments done at constant solution undersaturation are summarized in Table 6.

Table 6 Experimental conditions for the experiments done at variable undersaturation; total carbonate, C_t = 1.14 mM, pH 8.25, 25 °C, 0.1 M NaCl [36,47].

$Ca_t/1 \times 10^{-3}$ M	Rate of dissolution (Carrara marble)/ $\times 10^{-7}$ mol m^{-2} s^{-1}	Undersaturation $\sigma_{\text{Carrara marble}}$	σ_{calcite}	Rate of dissolution (calcite)/ $\times 10^{-7}$ mol m^{-2} s^{-1}
1.250	3.1	0.564	0.013	2.2
1.200	4.5	0.573	0.053	2.5
1.150	4.7	0.582	0.074	2.7
1.100	4.7	0.596	0.106	3.5
1.025	5.8	0.605	0.134	3.7
0.960	6.1	0.618	0.172	4.4
0.877	6.8	0.634		

The kinetics of dissolution for the two solids is shown in Fig. 17.

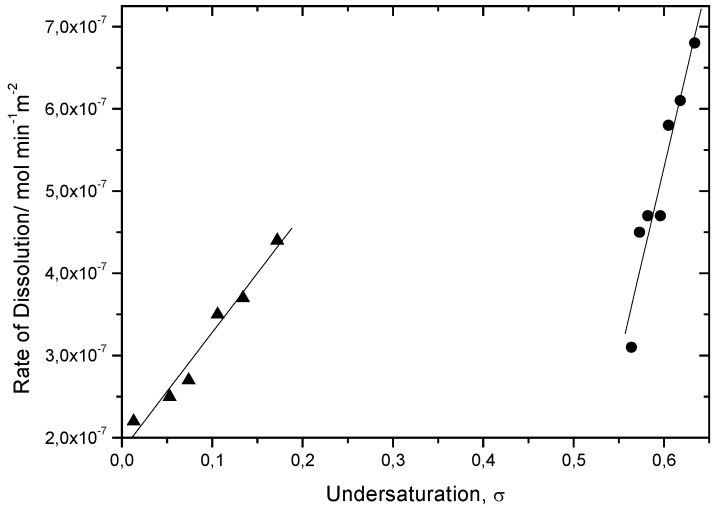

Fig. 17 Rate of dissolution as a function of the solution undersaturation, 25 °C, 0.10 M NaCl. (▲): calcite; (●): Carrara marble.

As may be seen in Fig. 17, although the dissolution experiments were done at identical solution conditions, the kinetics of dissolution was markedly different because of the large difference of the respective driving forces. The first-order dependence in the range of undersaturations examined in combination with the independence of the kinetics of dissolution on the fluid velocity, suggested that the rate-determining step in the dissolution is the surface diffusion of the building blocks from the surface of the dissolving crystals. The surface control of the dissolution suggests that compounds that through ionization may form surface complexes with the calcitic surface have higher chances to block the active sites and act as dissolution inhibitors. It is also interesting to note that the comparison of the rates of dissolution of the two calcitic materials showed that a certain value is attained at significantly lower undersaturation for calcite (i.e., closer to equilibrium) in comparison with the corresponding undersaturation with respect to the marble material. An additional factor contributing to the marked difference between the crystal dissolution rates of calcite and calcitic marble is the inhomogeneity of the particles involved. Marble grains consisted of large particles (ca. 200 μm) with a large number of much smaller particles attached, as seen in Fig. 18a. Exposure to the undersaturated solutions is followed by a rapid dissolution stage during which the smaller particles are eliminated (Fig. 18b). It is very likely that size-dependent solubility differences contribute to this effect. Since the Carrara marble dissolution process was found to be controlled by surface diffusion, we attempted to treat the surface by compounds which may either adsorb on the surface or form surface complexes. The organophosphorus compound (1-hydroxyethylidene)-1,1-diphosphonic acid (HEDP) was thus tested. It was found that HEDP adsorbed at the surface of Carrara marble and, as a result, considerable rate of dissolution reduction was recorded [47], as in Fig. 19 even at concentrations as low as 1 μM. Measurements of the surface charge of the Carrara marble, showed that at the experimental conditions used, the surface was positively charged, thus favoring electrostatic interactions in addition to surface complexation [47].

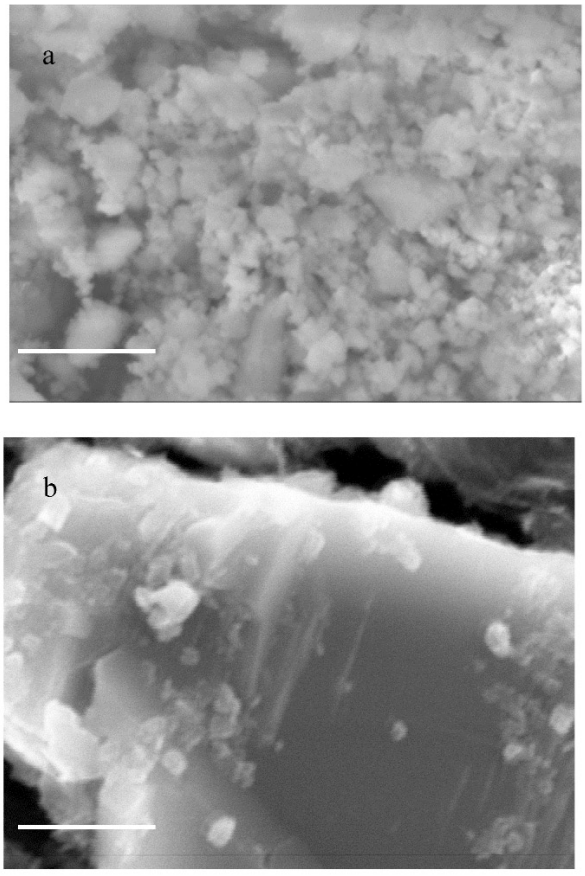

Fig. 18 Carrara marble: (a) before dissolution (bar is 5 μm); (b) after dissolution (bar 3 μm) at pH 8.25, 25 °C, 0.1 M NaCl.

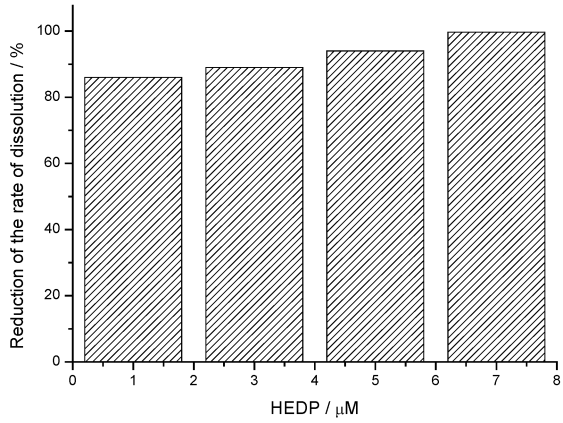

Fig. 19 Inhibition of the rate of dissolution of the Carrara marble in the presence of HEDP; pH 8.25, 25 °C, $\sigma = 0.634$.

CONCLUSIONS

Crystal growth and dissolution processes are very important in numerous applications from biological mineralization to scale formation and the deterioration of building materials. The rate of formation of the various minerals and the stability of intermediate crystalline phases depends on the solution supersaturation and the relative solubility of the various phases. In the calcium phosphate system, intermediate phases may be stabilized kinetically. The identification of intermediate phases and/or their formation near the solubility limit may be investigated from supersaturated solutions, regardless of the degree of supersaturation by keeping the supersaturation constant. Heterogeneous nucleation studies even at low supersaturations may be carried out, revealing the nucleation capacity of foreign substrates introduced in supersaturated solutions. The calcification of heart valve prostheses is a typical example. Porcine heart valves used as substrates showed the propensity of the collagenous tissues for the nucleation and growth of calcium phosphates. The mineral forming depends largely on the solution supersaturation. The constant supersaturation methodology allows for the precipitation of solids at steady-state conditions. In the case of magnesium ammonium phosphate (struvite), the precipitation of the solid may be investigated over a wide supersaturation range so that both the stability diagram of the system and the kinetics of the formation of the solid may be investigated with high reproducibility from media as complicated as wastewater. Finally, the solubility limit of sparingly soluble salts is very important for understanding the dissolution mechanism underlying the damage of materials. The case of calcitic marble (Carrara) was presented. The solubility of this material measured showed marked differences in comparison with the principal component, calcite. The dissolution rates were measured at constant undersaturation, and the prevalent mechanism was found to be surface diffusion of the calcite crystals building blocks. The presence of compounds with functional groups that may be ionized in solution resulted in the inhibition of the rates of dissolution at very low concentrations.

REFERENCES

1. J. C. Cowan, D. J. Weintritt. *Water Formed Scale Deposits*, p. 204, Gulf Publishing, Houston (1976).
2. A. S. Myerson. In *Handbook of Industrial Crystallization*, A. S. Myerson (Ed.), pp. 1–31, Butterworth-Heinemann, Boston (1993).
3. J. W. Mullin. *Crystallization*, 3rd ed., pp. 118–122, Butterworth-Heinemann, Oxford (1993).
4. N. W. Cayes, J. Estrin. *Industrial and Engineering Chemistry Fundamentals* **6**, 13 (1967).
5. J. Garside, R. J. Davey. *Chem. Eng. Commun.* **4**, 393 (1980).
6. C. W. Davies. *Ion Association*, Butterworths, London (1962).
7. K. S. Pitzer. In *Activity Coefficients in Electrolyte Solutions*, Vol. 1, R. M. Pytkowitz (Ed.), pp. 157–208, CRC Press, Boca Raton (1979).
8. J. W. Ball, D. K. Nordstrøm. *WATEQ4F-User's manual with Revised Thermodynamic Data Base and Test Cases for Calculating Speciation of Major, Trace and Redox Elements in Natural Waters*, p. 185, U.S. Geological Survey Open File Report 90-129 (1991).
9. D. K. Nordstrøm, L. N. Plummer, T. M. L. Wigley, T. J. Wolery, J. W. Ball, E. A. Jenne, R. L. Basset, D. A. Crerar, T. M. Florence, B. Fritz, M. Hoffman, G. R. Holdren, G. M. Lafon, S. V. Mattigod, R. E. McDuff, F. Morel, M. M. Reddy, G. Sposito, J. Thrailkill. In *Chemical Modelling in Aqueous Systems. Speciation, Solubility and Kinetics*, E. A. Jenne (Ed.), pp. 857–892, ACS Symposium Series No. 93, American Chemical Society, Washington, DC (1979).
10. G. H. Nancollas. *Interactions in Electrolyte Solutions*, Elsevier, Amsterdam (1965).
11. J. W. Mullin, M. Chakraborty, Mehtak. *J. Appl. Chem.* **13**, 423 (1970).
12. G. D. Botsaris, E. G. Denk, J. Chua. *AIChE Symp. Ser. No. 121*, **68**, 21 (1972).
13. I. X. Malollari, P. G. Klepetsanis, P. G. Koutsoukos. *J. Cryst. Growth* **155**, 240 (1995).
14. W. K. Burton, N. Cabrera, F. C. Frank. *Philos. Trans. R. Soc. London* **243**, 299 (1951).

15. A. E. Nielsen. *J. Cryst. Growth* **67**, 289 (1984).
16. G. H. Nancollas. In *Biomineralization*, S. Mann, J. Weloto, R. J. P. Williams, (Eds.), pp. 157–187, VCH, New York (1989).
17. M. Volmer. *Kinetic der Phasenbildung*, Steinkopff, Leipzig (1939).
18. A. E. Nielsen, J. M. Toft. *J. Cryst. Growth* **67**, 278 (1984).
19. A. A. Chernov. *Soviet Physics Uspekhi* **4**, 116 (1961).
20. M. O'Hara, R. C. Reid. *Modelling Crystal Growth Rates from Solution*, Prentice Hall, New York (1973).
21. E. A. Eanes, I. H. Gillessen, A. S. Posner. *Nature* **208**, 365 (1965).
22. H. Newesely. *Arch. Oral Biol.* **6**, 174 (1966).
23. F. Betts, A. S. Posner. *Mater. Res. Bull*. **9**, 907 (1974).
24. H. Furedi-Milhofer, B. Purgaric, L. Brecevic, N. Pavkovic. *Calcif. Tissue Res.* **8**, 142 (1971).
25. G. H. Nancollas, B. Tomazic. *J. Phys. Chem.* **78**, 2218 (1974).
26. M. D. Francis, N. C. Webb. *Calcif. Tissue Res.* **6**, 335 (1971).
27. N. Spanos, P. G. Koutsoukos. *J. Phys. Chem. B* **102**, 6679 (1998).
28. G. H. Nancollas. In *Biomineralization*, S. Mann, J. Webb, R. J. P. Williams, (Eds.), pp. 157–187, VCH, Weinheim (1989).
29. J. P. Barone, G. H. Nancollas. *J. Colloid Interface Sci.* **62**, 421 (1977).
30. J. Garside, L. G. Gibilaro, N. S. Tavare. *Chem. Eng. Sci.* **37**, 1625 (1982).
31. M. B. Tomson, G. H. Nancollas. *Science* **200**, 1059 (1978).
32. P. G. Koutsoukos, Z. Amjad, M. B. Tomson, G. H. Nancollas. *J. Am. Chem. Soc.* **102**, 1553 (1980).
33. N. Bouropoulos, P. G. Koutsoukos. *J. Cryst. Growth* **213**, 381 (2000).
34. A. N. Kofina, P. G. Koutsoukos. *Cryst. Growth Des.* **5**, 489 (2005).
35. T. F. Kazmierczak, M. B. Tomson, G. H. Nancollas. *J. Phys. Chem.* **86**, 103 (1982).
36. M. Orkoula, P. G. Koutsoukos. *Langmuir* **16**, 7263 (2000).
37. NIST Standard Reference Database 46, Version 6.0, NIST Standard Reference Data, Gaithersburg, MD (2001).
38. T. Kokubo, H. Kushitani, S. Sakka, T. Kitsugi, T. Yamamuro. *J. Biomed. Mater. Res.* **24**, 721 (1990).
39. E. I. Dorozhkina, S. V. Dorozhkin. *Colloids Surf., A* **223**, 231 (2003).
40. S. V. Dorozhkin, E. I. Dorozhkina. *Colloids Surf., A* **215**, 191 (2003).
41. J. Lyklema. *Pure Appl. Chem.* **63**, 895 (1991).
42. S. W. Massey. *Sci. Total Environ.* **227**, 109 (1999).
43. R. N. Butlin, A. T. Coote, M. Devenish, I. F. C. Hughes, C. M. Hutchens, J. G. Irwin, T. J. Yates. In *Proceedings of the 17th International Congress on Deterioration and Conservation of Stone*, J. Delgado-Rodrigues, F. Henriques, F. Telma Jeremias (Eds.) pp. 345–353, Portugal, Lisbon (1992).
44. A. E. Charola. *Durability Building Mater*. **5**, 309 (1988).
45. K. L. Gauri, S. S. Tambe, E. N. Caner-Saltik. *Environ. Geol. Water Sci.* **19**, 55 (1992).
46. A. Arnold. In *Proceedings of European Commission Research Workshop: Origin Mechanisms and Effects of Salts on Degradation of Monuments in Marine and Continental Environments*, F. Zezza (Ed.), pp. 20–25, Bari, Italy (1996).
47. D. G. Kanellopoulou, P. G. Koutsoukos. *Langmuir* **19**, 5691 (2003).
48. L. N. Plummer, T. M. I. Wigley, D. L. Parkhurst. *Am. J. Sci.* **278**, 179 (1978).